Electronic Supplementary Material (ESI) for Physical Chemistry Chemical Physics.

Ferroelectric and strain-tuned $MoSe_2/Bi_2O_2Se$ van der Waals heterostructure with band alignment evolution

Shucao Lu[a], Yanlu Li[a,*], Xian Zhao[b,*]

[a]State Key Laboratory of Crystal Materials and Institute of Crystal Materials, Shandong University, Jinan, 250100, China

[b]Center for Optics Research and Engineering of Shandong University, Shandong University, Qingdao, 266237, China

Corresponding authors:

Y. L. Li email: liyanlu@sdu.edu.cn

X. Zhao email: xianzhao@sdu.edu.cn

Supporting Information

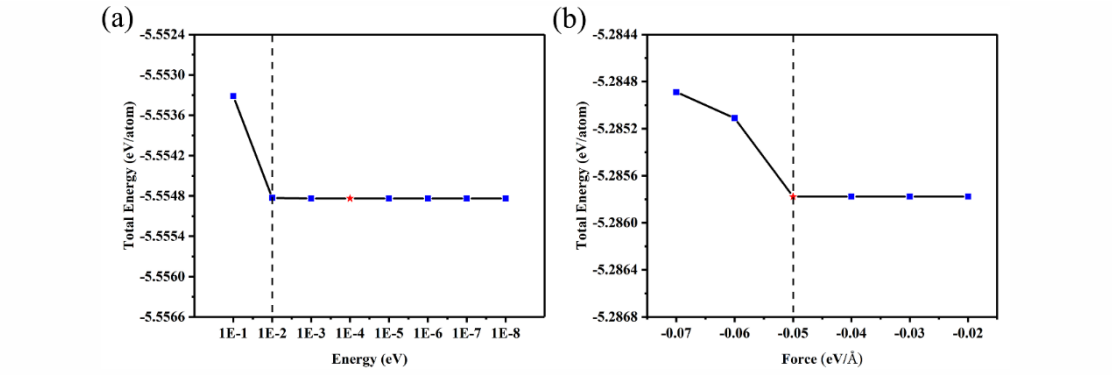

Fig. S1. Convergence tests for energy (a) and force (b), respectively.

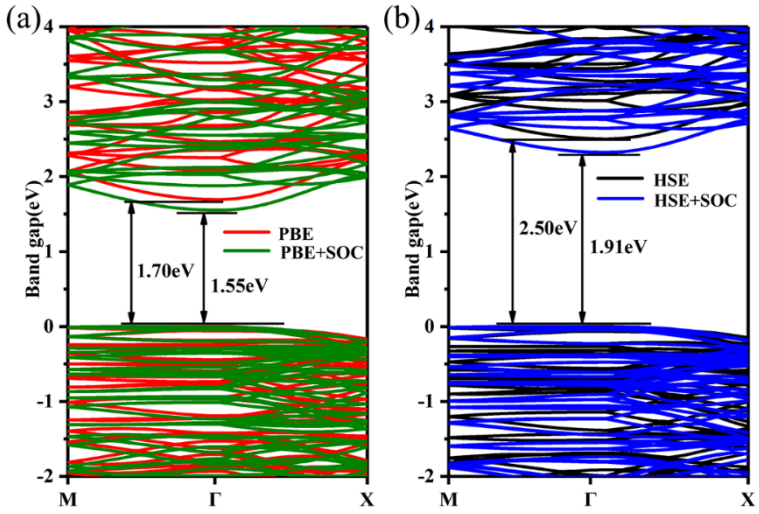

Fig.S2. Band structures of the Bi_2O_2Se monolayer (zipper surface model with 3×4 supercell) with (a) PBE, PBE+SOC and (b) HSE, HSE+SOC approaches.

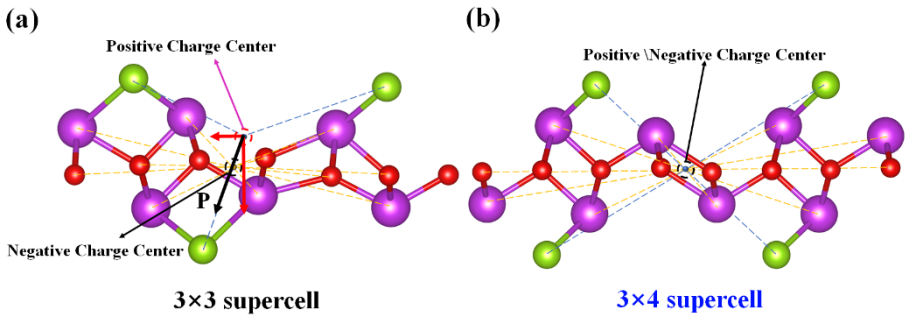

Fig.S3. Positive and negative charge centers of 3×3 (a) and 3×4 (b) Bi_2O_2Se monolayers.

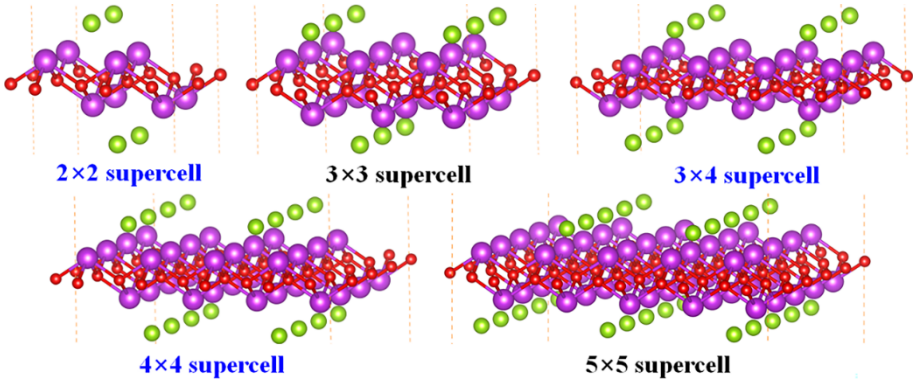

Fig.S4. Crystal structures of the Bi_2O_2Se monolayer with 2×2, 3×3, 3×4 , 4×4 and 5×5 supercells.

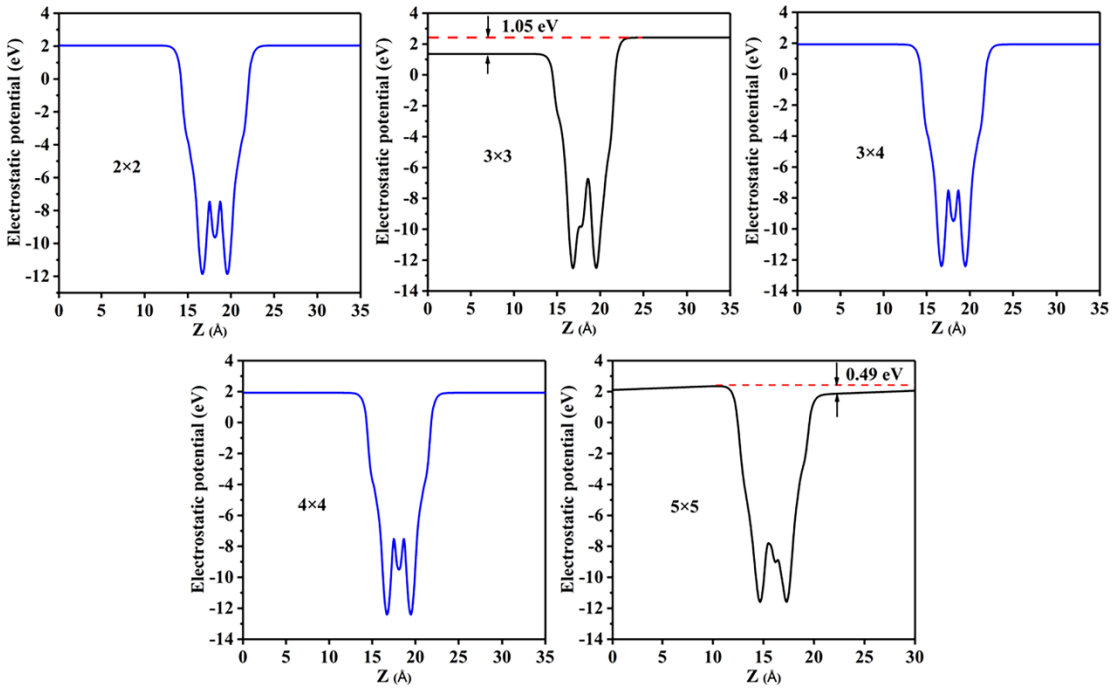

Fig.S5. Electrostatic potentials of the Bi_2O_2Se monolayer with 2×2, 3×3, 3×4 , 4×4 and 5×5 supercells.

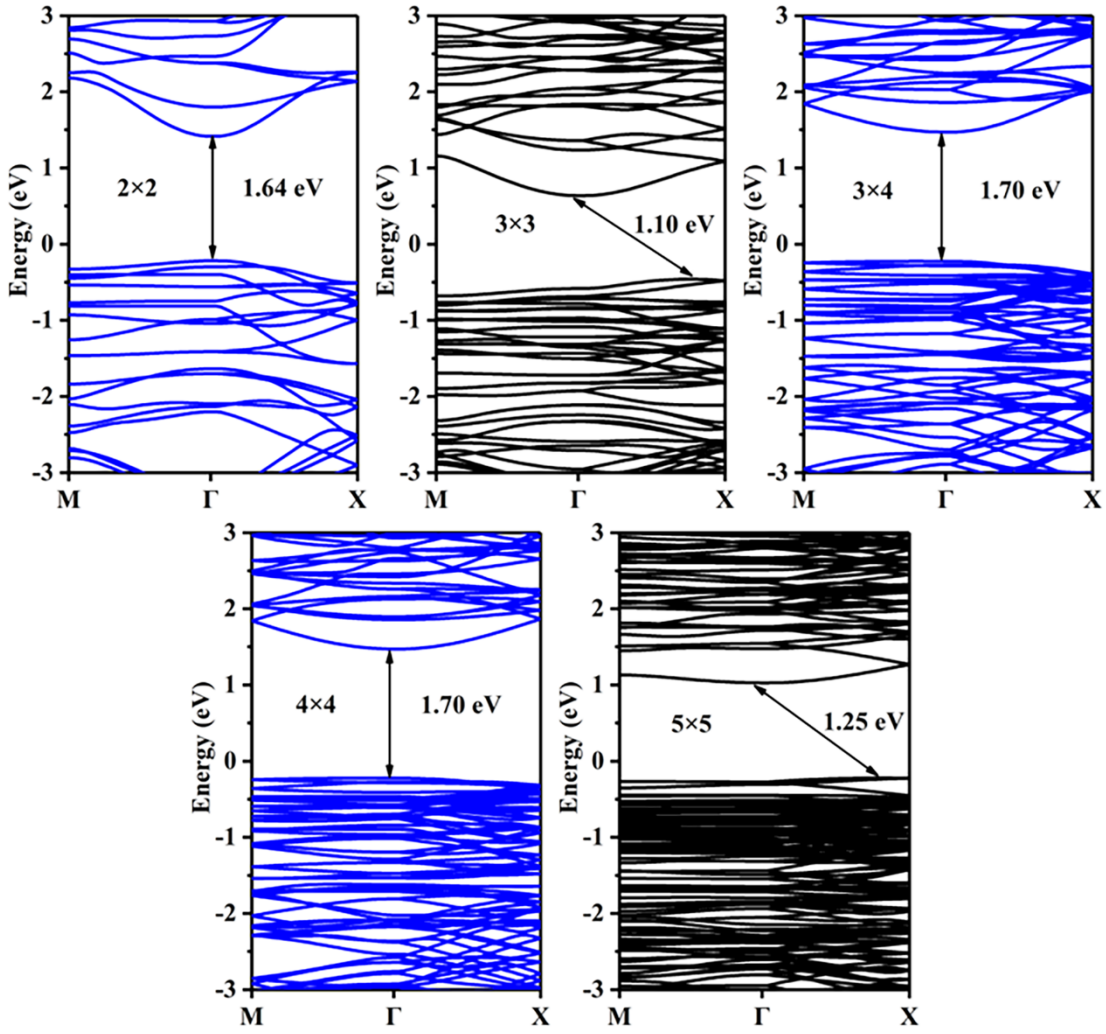

Fig.S6. Band structures of the Bi_2O_2Se monolayer with 2×2, 3×3, 3×4 , 4×4 and 5×5 supercells. The Fermi level is set to zero.

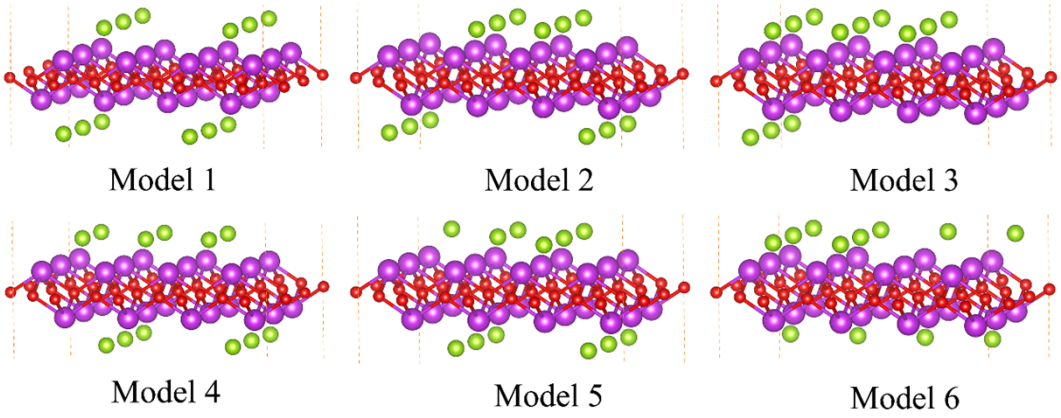

Fig.S7. Crystal structures of the considered Bi_2O_2Se monolayer models.

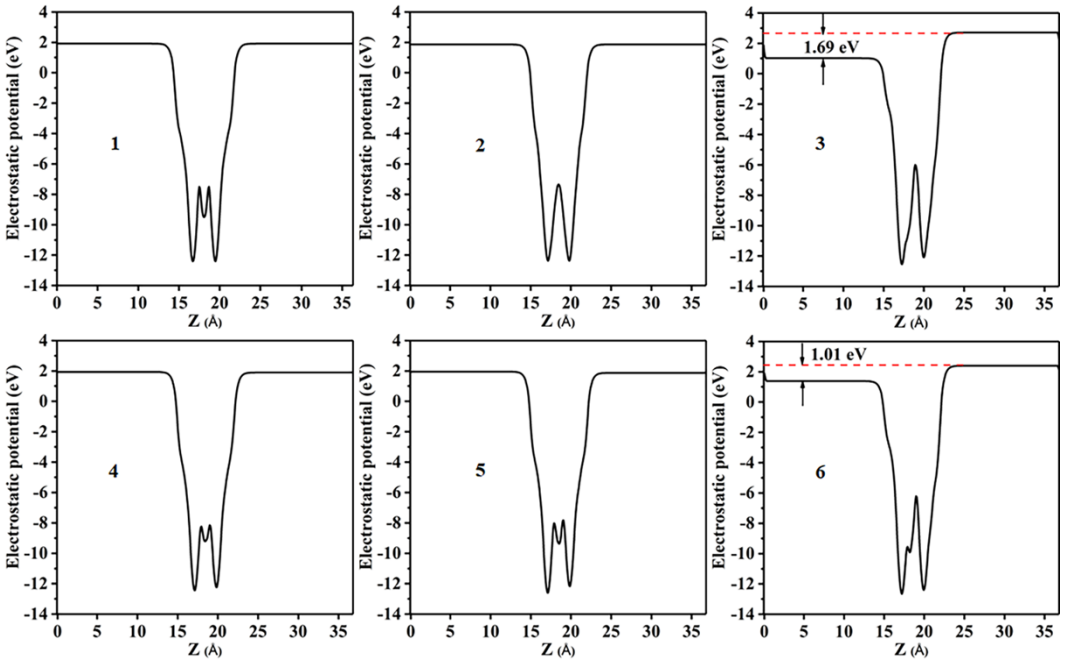

Fig.S8. Electrostatic potentials of the considered Bi_2O_2Se monolayer models.

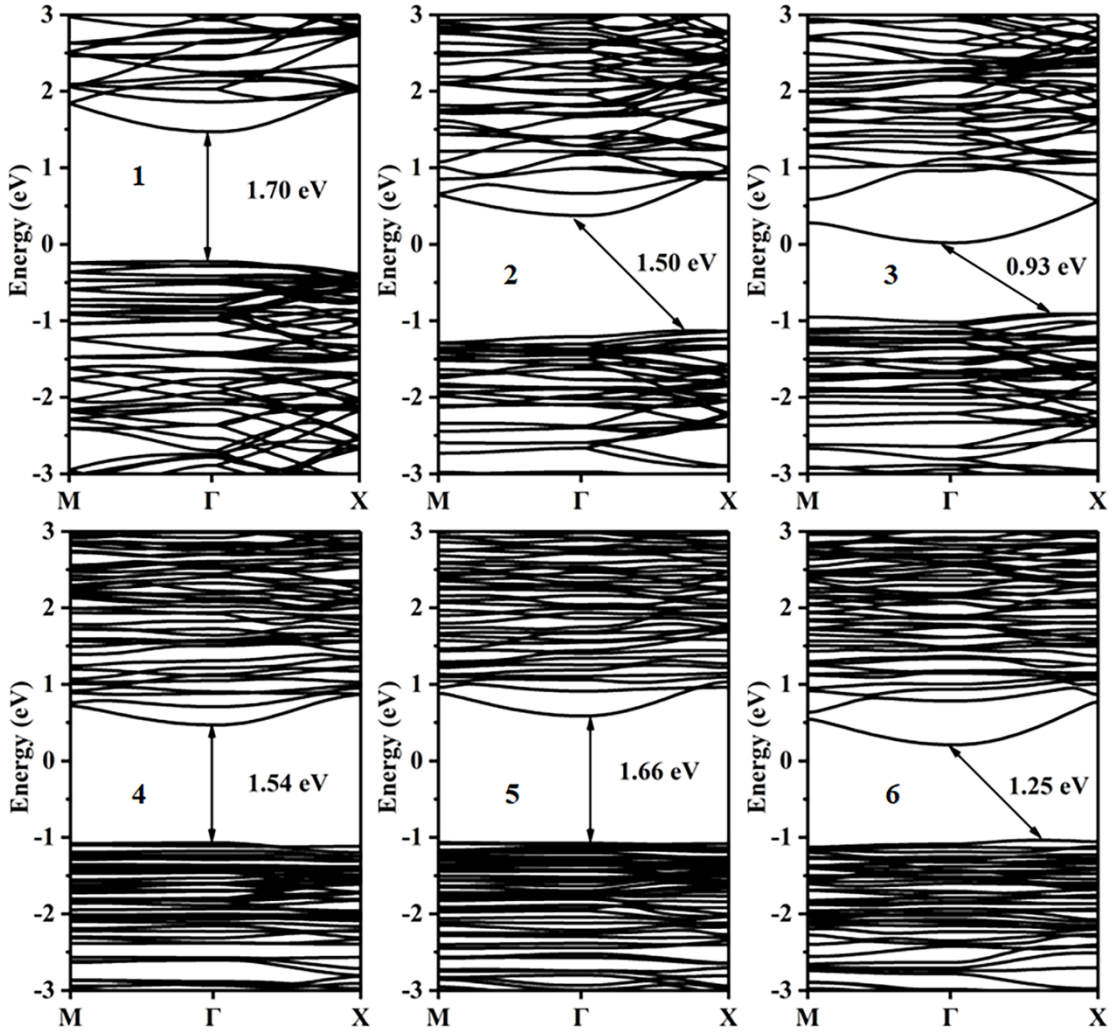

Fig.S9. Band structures of the considered Bi_2O_2Se monolayer models. The Fermi level is set to zero.

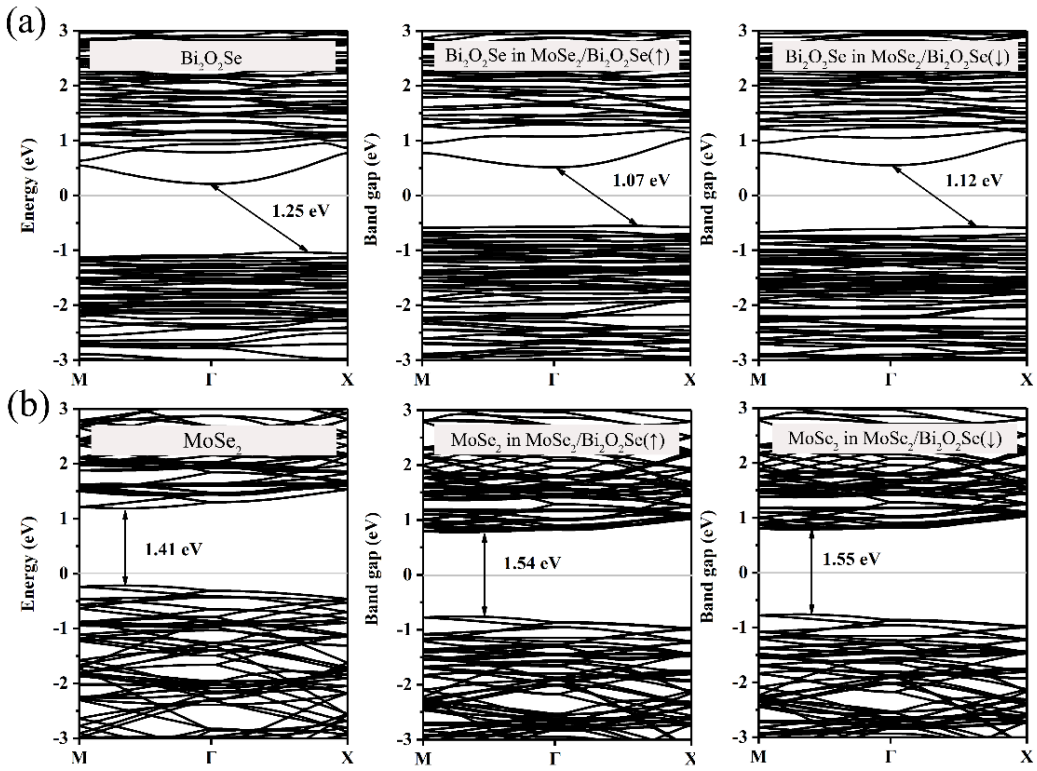

Fig. S10. Band structures of Bi_2O_2Se and those in $MoSe_2/Bi_2O_2Se(\uparrow)$ and $MoSe_2/Bi_2O_2Se(\downarrow)$ (a), as well as $MoSe_2$ and those in $MoSe_2/Bi_2O_2Se(\uparrow)$ and $MoSe_2/Bi_2O_2Se(\downarrow)$ (b).

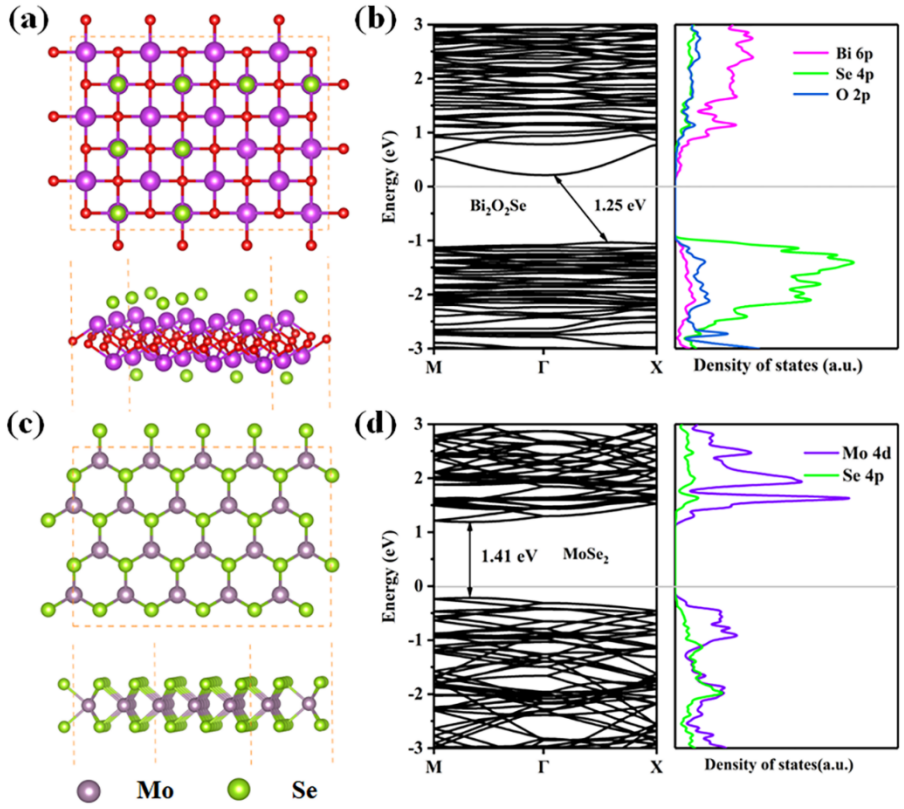

Fig.S11. Top- and side-view of the crystal structures, band structures and projected density of states of (a, b) Bi_2O_2Se and (c, d) $MoSe_2$. The Fermi level is set to zero.

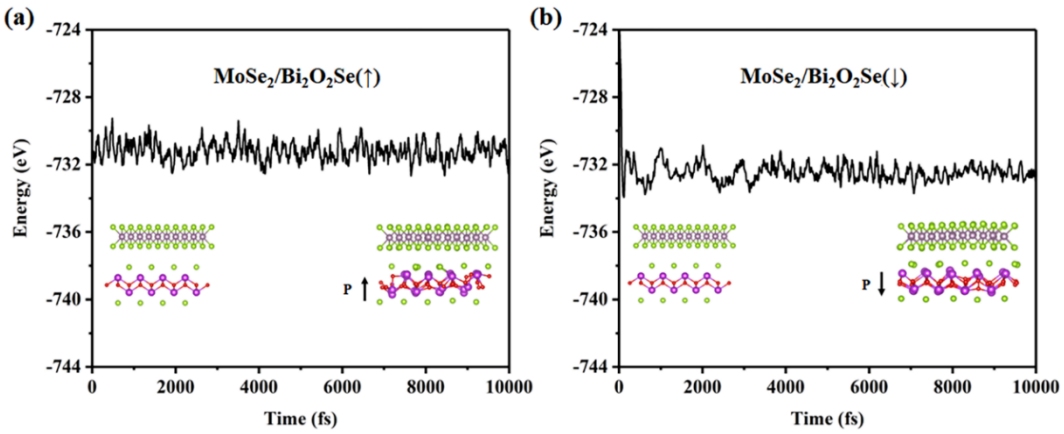

Fig.S12. Variation of the total energies of (a) $MoSe_2/Bi_2O_2Se(\uparrow)$ and (b) $MoSe_2/Bi_2O_2Se(\downarrow)$ at 300 K. The structures before and after the evolution of 10 ps are also shown.

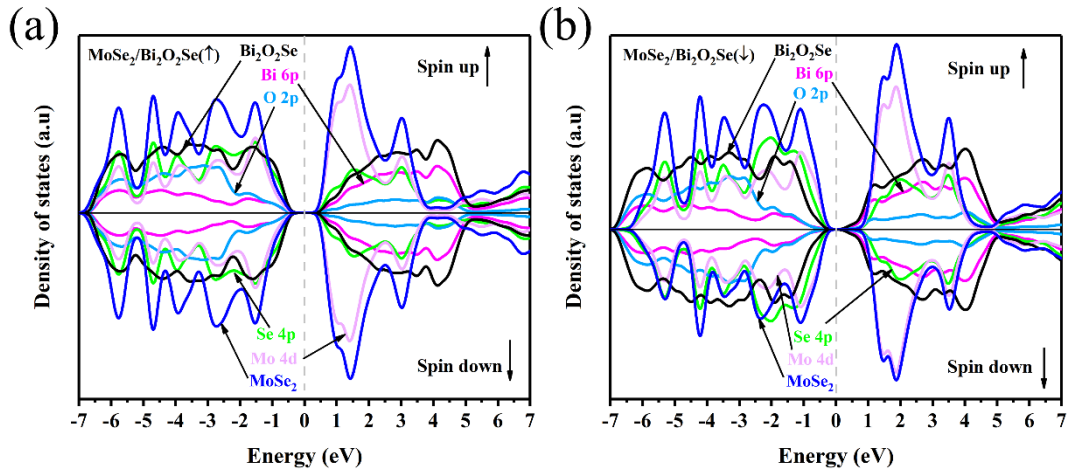

Fig. S13. Spin density of states of $MoSe_2/Bi_2O_2Se$ (↑) and $MoSe_2/Bi_2O_2Se$ (↓).

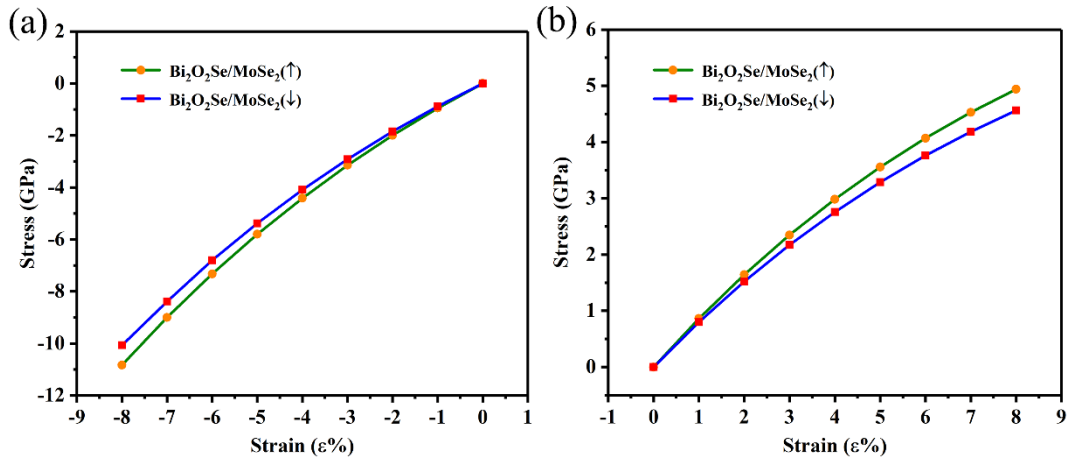

Fig. S14. The curve of stress vs. strain of the heterostructure under tensile strain (a) and compressive strain (b).

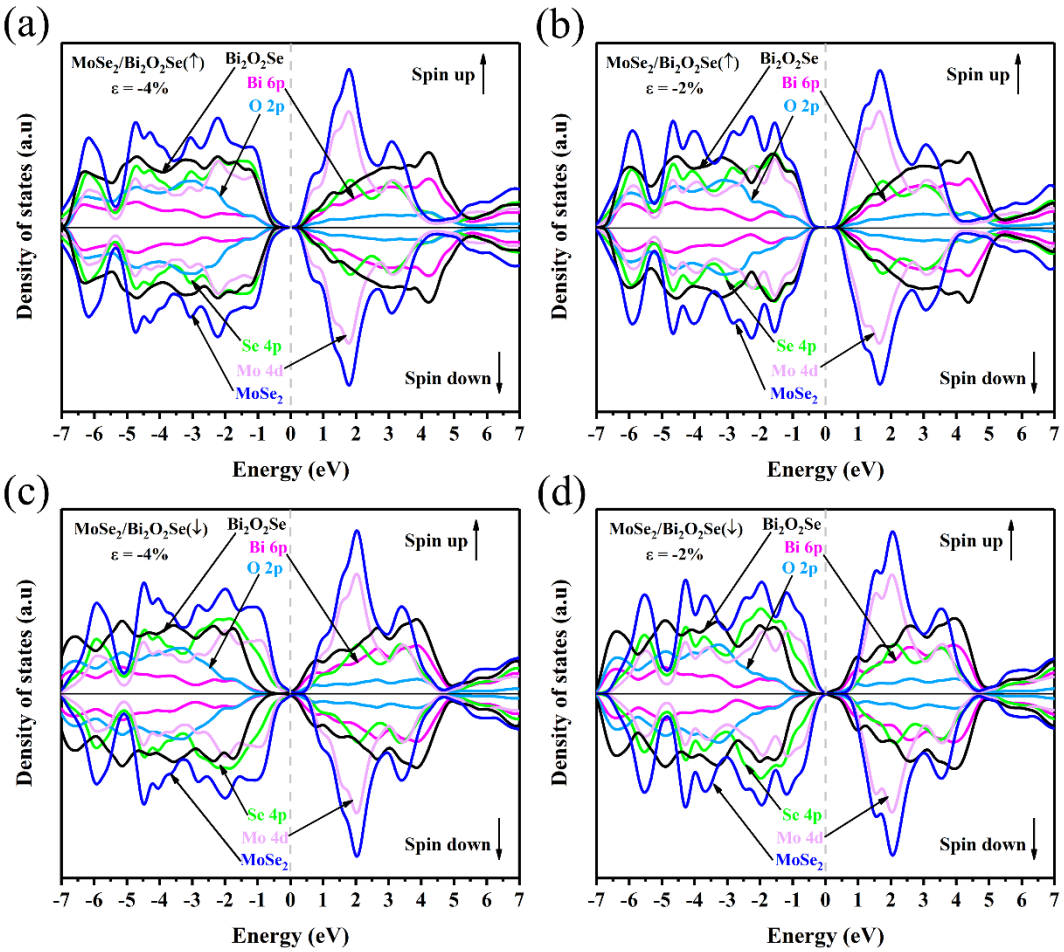

Fig. S15. Spin density of states of $MoSe_2/Bi_2O_2Se$ (↑) under the in-plane strain of (a) ε = -4% and (b) ε= -2%, and of $MoSe_2/Bi_2O_2Se$ (↓) under the in-plane strain of (c) ε = -4% and (d) ε= -2%.

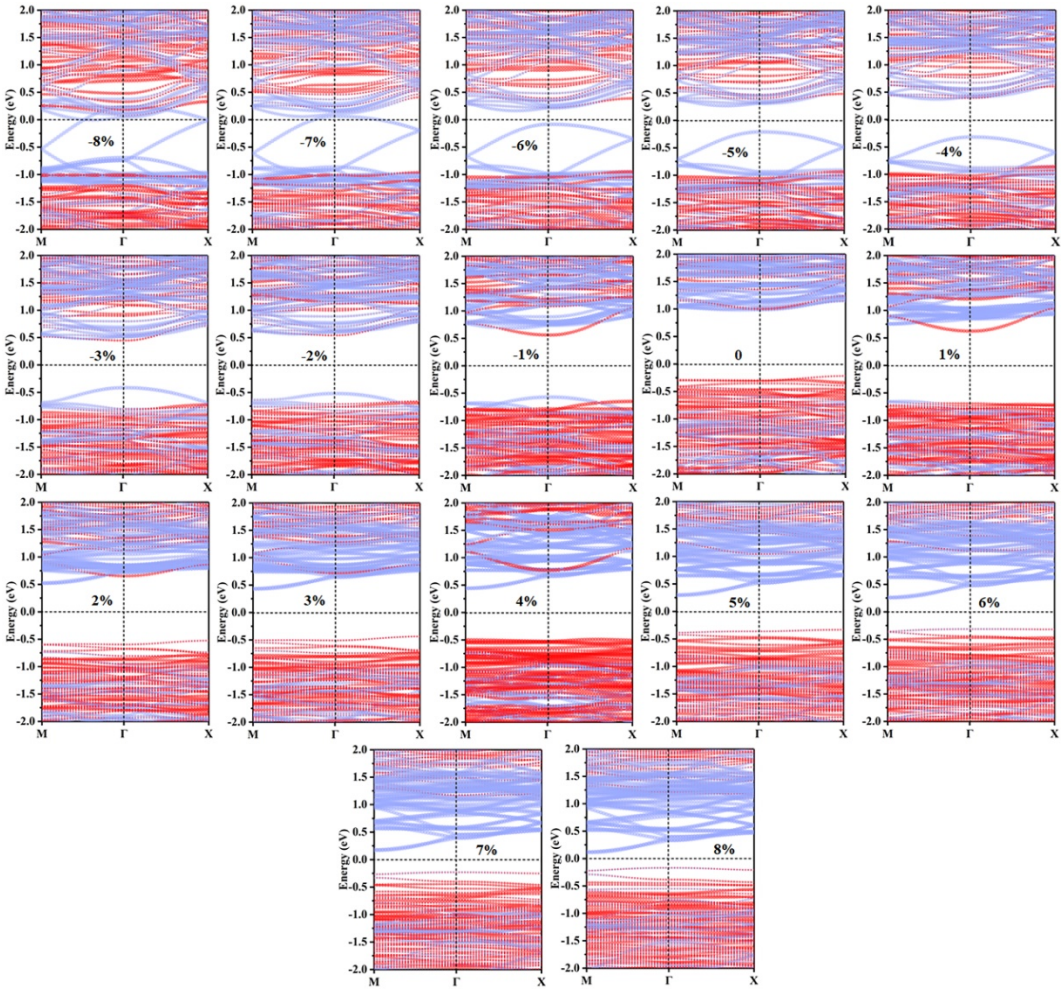

Fig. S16. Projected band structures of $MoSe_2/Bi_2O_2Se(\uparrow)$ under different in-plane strain. The Fermi level set to be zero. Red and blue dots represent the contributions of Bi_2O_2Se and $MoSe_2$ layers, respectively.

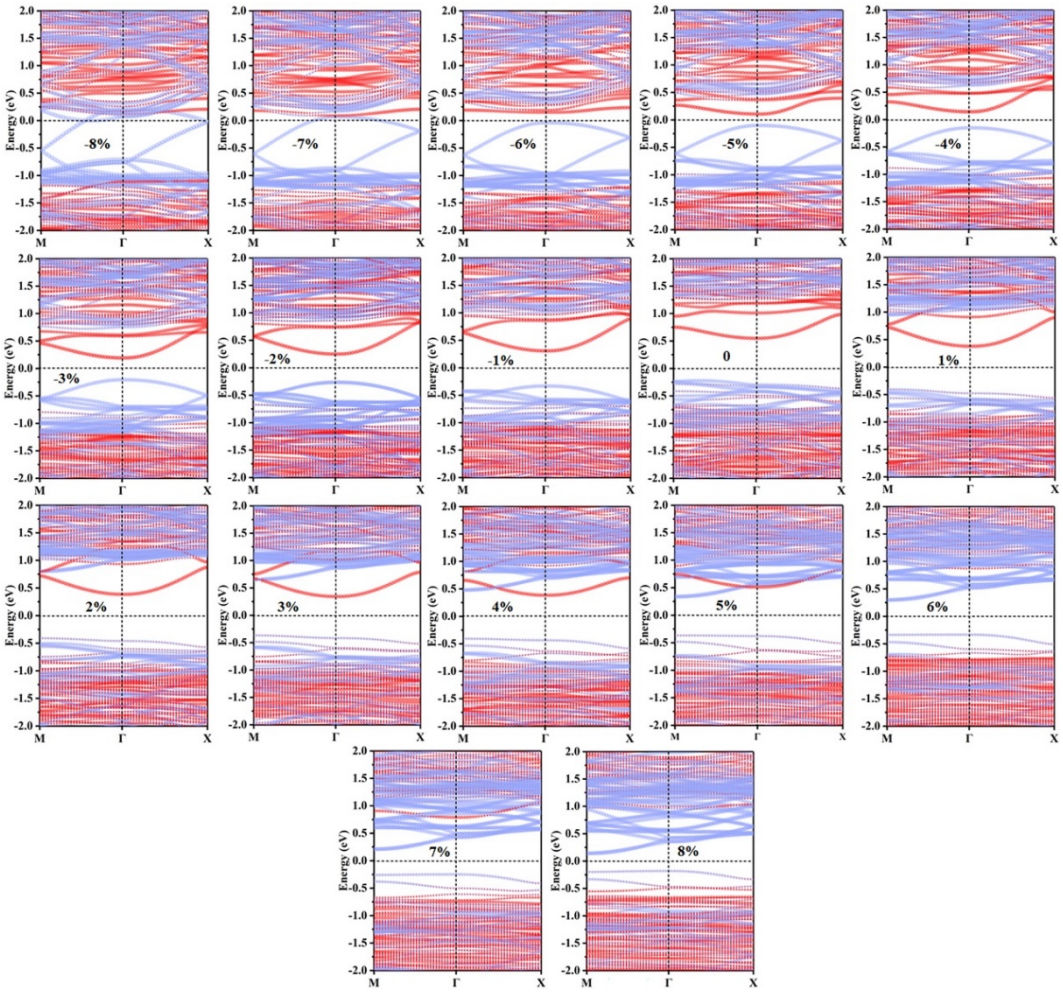

Fig. S17. Projected band structures of $MoSe_2/Bi_2O_2Se(\downarrow)$ under different in-plane strain. The Fermi level set to be zero. Red and blue dots represent the contributions of Bi_2O_2Se and $MoSe_2$ layers, respectively.

Table S1. Formation energies (eV/atom) of 6 different Bi_2O_2Se monolayer models

	Formation energy (eV/atom)
Model 1	-0.912
Model 2	-0.891
Model 3	-0.882
Model 4	-0.897
Model 5	-0.901
Model 6	-0.895

Table S2. Binding energies E_b of the considered Bi_2O_2Se monolayer models in Fig. S7.

	E_b (emV/Å^2)
Model 1	157.43
Model 2	164.33
Model 3	167.40
Model 4	162.77
Model 5	160.95
Model 6	163.07

Table S3. Bond lengths (Å) of Bi-Se in Bi_2O_2Se and Mo-Se in $MoSe_2$ as a function of biaxial strain for $MoSe_2/Bi_2O_2Se(\uparrow)$ and $MoSe_2/Bi_2O_2Se(\downarrow)$

	$MoSe_2/Bi_2O_2Se(\uparrow)$		$MoSe_2/Bi_2O_2Se(\downarrow)$	
	d_{Bi-Se}	d_{Mo-Se}	d_{Bi-Se}	d_{Mo-Se}
-8%	2.748	2.475	2.697	2.485
-6%	2.758	2.473	2.826	2.514
-4%	2.863	2.493	2.735	2.496
-2%	2.990	2.496	2.808	2.512
0%	3.019	2.518	2.883	2.529
2%	3.012	2.574	2.905	2.527
4%	3.173	2.600	2.975	2.540
6%	3.128	2.630	3.001	2.551
8%	3.335	2.657	3.178	2.572